CONTROLLING THE RIDE HEIGHT OF HYDRO-FOILING BOATS IN RANSE CFD

F.M.J. Bergsma[1], K.S. Zaaijer[1], N. Moerke[1]

[1] Van Oossanen Naval Architects, Costerweg 1b, 670AA, Wageningen, Netherlands

ABSTRACT

High performance crafts include hydro foiling crafts. In many types of design the high performance nature and the fuel efficiency of foiling marine vehicles is employed to develop state of the art designs. One example is the Solar Challenge, a biannual race between solar powered boats. By obtaining a stable foiling mode top speeds and efficiency can be improved. By controlling the pitch of the foils, the stability of the foiling mode can be improved and therefore foils control strategies should be developed. These control strategies are to find a balance between the attitude and velocity of the vessel at one side, and the dynamically generated forces on the other side. A target ride height and attitude is to be achieved in a stable way. This paper presents a method to perform simulations of the transition of a vessel from displacement mode to a target ride height. The pitch of all foils of the vessel is controlled using a proportional controller implemented via an user defined code in a commercially available RANSE CFD package. Computational issues concerning the rotation of the foils and the large vertical movement of the vessel are addressed as well in this paper. The results for two control strategies are presented.

NOMENCLATURE

AGR	Adaptive Grid Refinement
CFD	Computational Fluid Dynamics
COG	Centre of Gravity
e_{Ry0}	error in trim of vessel
e_{Tz0}	error in rise of vessel
$K_{i_{aft}}$	integral gain for aft foil
$K_{i_{fwd}}$	integral gain for forward foil
$K_{p_{aft}}$	proportional gain for aft foil
$K_{p_{fwd}}$	proportional gain for forward foil
RANSE	Reynolds Averaged Navier-Stokes Equations
Rn_{aft}	pitch angle of aft foil
$Rn_{aft_{max}}$	upper bound of pitch angle of aft foil
$Rn_{aft_{min}}$	lower bound of pitch angle of aft foil
Rn_{fwd}	pitch angle of forward foil
$Rn_{fwd_{max}}$	upper bound of pitch angle of forward foil
$Rn_{fwd_{min}}$	lower bound of pitch angle of forward foil
$Ry0$	trim angle of vessel
$Ry0_{target}$	target trim angle
$Tz0$	Rise of vessel
$Tz0_{target}$	target translation in z-direction (ride height)
$\vec{g}$	gravitational acceleration
$\bar{\bar{I}}$	Unit tensor
K	turbulence kinetic energy
$\vec{n}$	outward bound normal vector
p	pressure field
S	control volume surface
$\bar{\bar{S}}$	mean strain rate tensor
$\vec{U}$	velocity field

$\vec{U}_d$	velocity of surface S
$\overrightarrow{u'}$	flow velocity fluctuation
V	control volume
μ_t	turbulent viscosity
ρ	density
$\bar{\bar{\tau}}$	stress tensor
$\bar{\bar{\tau}}_l$	viscous stress tensor
$\bar{\bar{\tau}}_t$	Reynolds stress tensor

1. INTRODUCTION

1.1 Hydro-foiling Boats

For over a century mankind has the possibility to rise out of the water using hydro-foiling boats. First efforts were made by Enrico Forlanini and John Thornycroft around the beginning of the 20th century. With development efforts by, among others, Alexander Graham Bell knowledge on the hydro-foiling boats increased. It was only after the 2nd World war that hydro-foiling boats were used in commercial and military applications.

The peak of the popularity of hydro foils in commercial and military applications was in the 1960s and 1970s. Since that moment the popularity has decreased. One of the reasons is the technical complexity of hydro-foiling boats. Advanced ride control is required for hydro-foiling boats with fully submerged foils. Currently the application of hydro foils has an increasing popularity in racing and high performance competitive environments.

1.2 Solar Boat Challenge

The hydro-foiling boat analysed in the current paper is a design for the DONG Energy Solar Challenge. This is the largest race for solar powered boats worldwide. The race is a 200 km long course in the province of Friesland in The Netherlands and the competition is between dozens of international teams that design and build their own solar powered boat particularly designed for this race (Dong Energy Solar Challenge, 2014a). Since hydrofoils were first used in the Solar challenge of 2010, more and more competitors are using foils to increase top speed and efficiency (Dong Energy Solar Challenge, 2014b)

1.3 Geometry

The studied hydro-foiling solar boat has an overall length of 7 meters and a width of 1.6 meters. The foil configuration consists of one fully submerged foil forward on two struts, and one foil aft on a single strut. Nacelles are placed at the intersection of the struts and foils to house hinging mechanisms. The majority of the load is carried by the forward foil. Each foil section is able to pivot independently in order to control ride height, dynamic trim and roll independently.

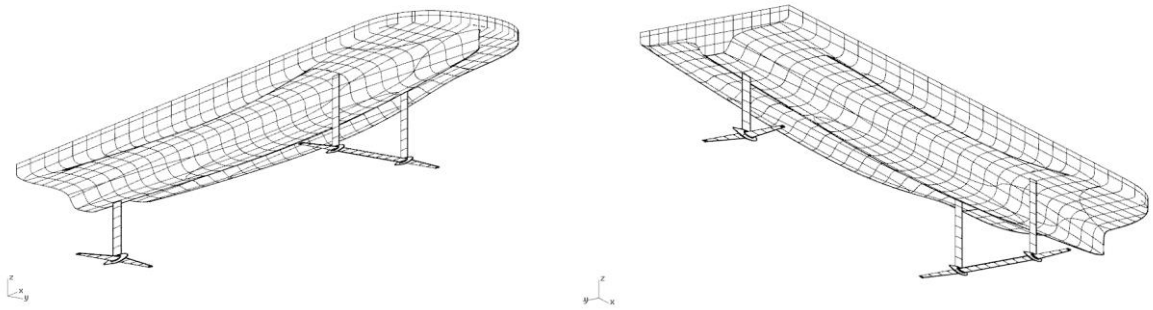

Fig. 1. Wire frame of the studied geometry.

The present study is aimed at introducing a method to study the control of the so called ride height and the trim of hydro-foiling vessels. Dynamic behaviour is simulated using established Computational Fluid Dynamics (CFD) methods. Pitch angles of the foils are adjusted during the simulation, using dynamic libraries that use the dynamic position of the vessel to adjust the foils orientations. First the employed method is described. Then the results obtained with the presented method for two control strategies are presented. In the final chapter the results are discussed and the conclusions are presented.

2. METHOD

This chapter provides the description of the methods applied for simulating a controlled ride height using a Computational Fluid Dynamics method. In section 2.1 details of the employed CFD method are given. In section 2.2 the control strategy is detailed.

2.1 Computational Fluid Dynamics Method

In this section a description is given of the CFD method used to determine the flow characteristics. The commercially available package FINE/Marine is used for generating the unstructured hexahedral mesh and solving the unsteady flow. In section 2.1.1 the governing equations are given. To enable the rotation of the foils of the hydro-foiling craft, a custom domain was generated. This is described in section 2.1.2. From this domain a mesh was generated. This is discussed in section 2.1.3. Adaptive refinement of the mesh is used to capture the water surface properly. The refinement of the water surface is discussed in section 2.1.4.

2.1.1. Governing equations

The modelling of the viscous flow is based on Reynolds Averaged Navier Stokes equations (RANSE) for incompressible unsteady flow. The equation for mass conservation is given in integral conservation form by:

$$\frac{\partial}{\partial t}\int_V \rho dV + \int_S \rho\left(\vec{U} - \vec{U}_d\right)\cdot\vec{n}dS = 0 \tag{1}$$

The equation of conservation of momentum is given by:

$$\frac{\partial}{\partial t}\int_V \rho\vec{U}dV + \int_S \rho\vec{U}\left[\left(\vec{U} - \vec{U}_d\right)\cdot\vec{n}\right]dS = \int_S \left(\bar{\bar{\tau}} - p\cdot\bar{\bar{I}}\right)\cdot\vec{n}dS + \int_V \rho\vec{g}dV \tag{2}$$

Closure of this set of equations is obtained by defining the stress tensor:

$$\bar{\bar{\tau}} = \bar{\bar{\tau}}_t + \bar{\bar{\tau}}_l \tag{3}$$

Here $\bar{\bar{\tau}}_t$ is the Reynolds stress tensor and $\bar{\bar{\tau}}_l$ the viscous stress tensor. The viscous stress tensor is defined as:

$$\bar{\bar{\tau}}_l = 2\mu\left(\bar{\bar{S}} - \frac{1}{3}\bar{\bar{I}}\,\vec{\nabla}\cdot\vec{U}\right) \tag{4}$$

The Reynolds stress tensor is given by:

$$\bar{\bar{\tau}}_t = -\rho\overrightarrow{\overrightarrow{u'}\cdot\overrightarrow{u'}} \tag{5}$$

A closure of this term is required to solve the set of equations. Turbulence viscosity models are used for this closure. These models are based on the Boussinesq approximation. This commonly used approximation gives the Reynolds stress as follows:

$$\bar{\bar{\tau}}_t = -\rho\overrightarrow{\overrightarrow{u'}\cdot\overrightarrow{u'}} = 2\mu_t\left(\bar{\bar{S}} - \frac{1}{3}\bar{\bar{I}}\,\vec{\nabla}\cdot\vec{U}\right) - \frac{2}{3}\rho K\bar{\bar{I}} \tag{6}$$

The near wall low Reynolds SST k-ω model of Menter (1993) was used. This is the recommended turbulence model for these kinds of computations (Numeca International, 2011).

2.1.2 Domain and Boundary Conditions

The domain around the hull is constructed such that the boundaries are far enough away to not influence the results. Using the symmetry from the centre-line, only half of the vessel was modelled. The dimensions of the computational domain around the hull are given in table 1. These are given relative to the reference point, which is at the intersection of the centreline, transom and water plane in hydrostatic condition.

Table 1. Domain size in meters relative to the reference point.

Direction	Minimum (m)	Maximum (m)
X (longitudinal)	-21.0	14.0
Y (beam)	0.0	14.0
Z (height)	-14.0	3.5

All hull surfaces had a no-slip boundary condition using wall functions to capture the boundary layer. In the symmetry plane a mirror boundary condition was applied and on the top and bottom of the domain the pressure was prescribed. All remaining domain faces have external/free-flow boundary conditions with a prescribed flow speed of v = 0 m/s.

The domain around each of the foils is constructed such that the foils can rotate around their span wise axis. Cylinder shaped domains are formed around the foils and all cylinders had a radius of 0.22 m. Their centreline was parallel to the y-axis and was collocated with the axis of rotation of the foil. In figure 2 the cylindrical domain around the foil is given as generated inside the domain around the hull.

All surfaces of the foils had a no-slip boundary condition using wall functions to capture the boundary layer. In the symmetry plane a mirror boundary condition was applied. All other surfaces of the cylinder are coupled with the box shaped domain by means of sliding grids.

The box shaped domain around the hull (as described earlier) has cylinder-shaped recesses at the locations of the cylindrical domains around the foils. The surfaces that form the recess are

coupled with the cylinders by means of sliding grids. This method to connect the domains, allow the foils to pitch, within the main domain while keeping a coupling between the domains. The sliding grid approach was validated using submerged propellers (Queutey et al, 2011a) (Queutey et al, 2011b) and a self-propulsion computation with a rotating propeller (Visonneau et al, 2011).

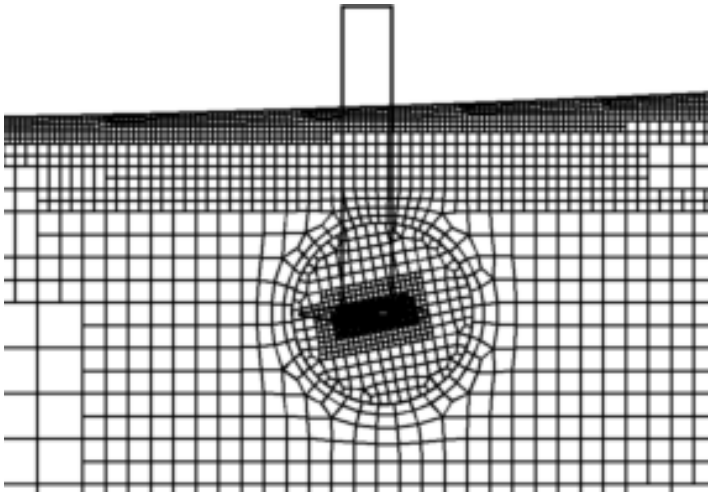

Fig. 2. Cylindrical mesh around the foil.

2.1.3 Computational Mesh

In this paragraph details of the unstructured mesh on the surface of the geometry are given. The domain volume is divided into small cells to generate the mesh. The largest cells on the hull are approximately $\Delta(X,Y,Z) \approx 0.0275$ m in size. In areas with large curvature and detailed flow phenomena, cells as small as $\Delta(X,Y,Z) \approx 0.00085$ m were used to ensure that flow features have a good resolution. The first cell near the wall was set to have a size of approximately 0.00033 m, such that its non-dimensional distance (y+) to the wall was approximately 29.6.

In order to have the best possible data transfer between the cylindrical domains around the foils and the cubic domain around the vessel via the sliding grid method, the mesh density (i.e. the cell size) was refined to be similar at both sides of the domain interface of the sliding grid. This leads to a mesh with approximately 4.3 million cells.

2.1.4 Refinement of mesh at free surface

Cells near the air-water interface were refined to have a size of 0.017 m in z-direction. These refinements are not included in the mesh a priori but are updated during the computation via Adaptive Grid Refinement (AGR). The cells that intersect with the free surface are further refined to the criterion mentioned above. Cells that do not intersect with the free surface anymore are de-refined (Wackers et al, 2012).

Initially the free surface is not refined at all. Therefore a very aggressive AGR strategy is used in the first 6 iterations in order to capture the free surface properly. Every time step the AGR method is called to make sure the mesh is sufficiently detailed to capture the free surface when the boat is accelerating.

The AGR method is used in order to allow a large rise of the vessel. Non-adaptive meshing strategies for capturing the free surface would move with the rising vessel causing the mesh to deform strongly. This negatively influences the stability of the computation. In addition the free surface refinement would not be at the location of the actual free surface. This would

decrease the accuracy of capturing the free surface. Figure 3 and 4 show the adaption of the mesh to the water surface, while the vessel is rising.

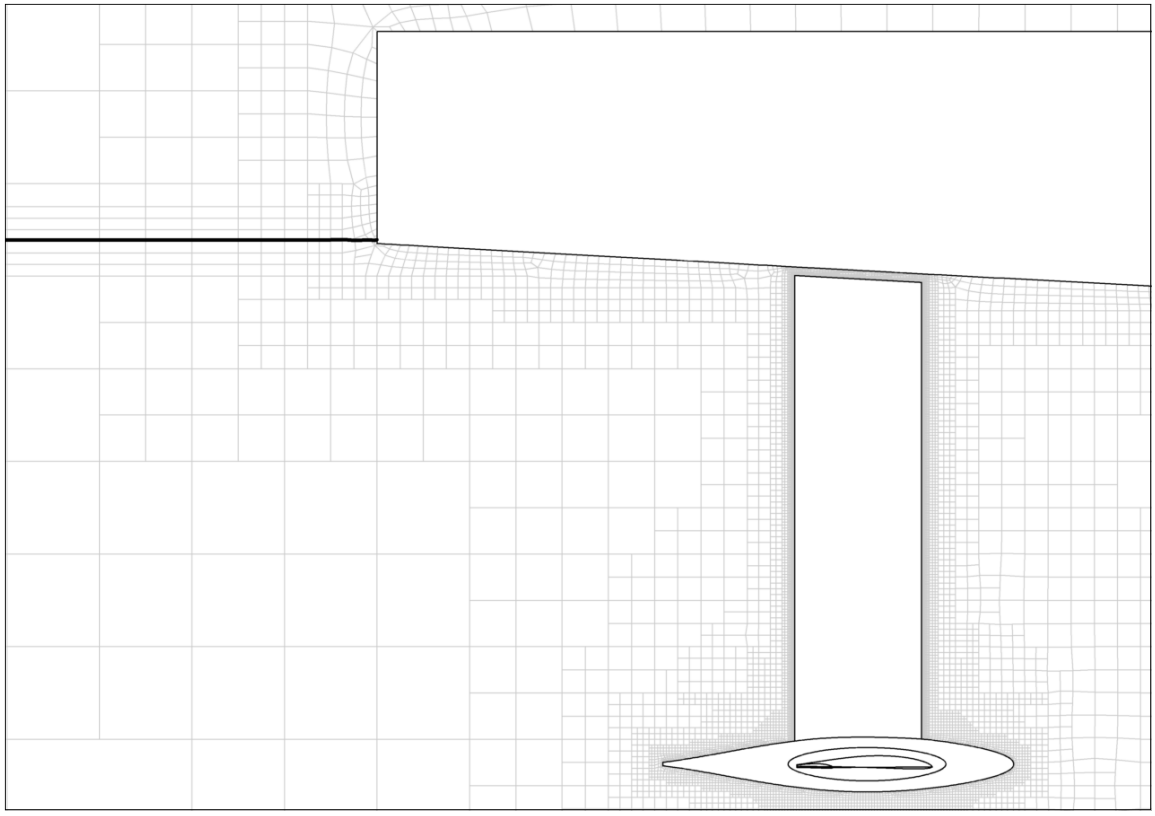

Fig. 3. The mesh at the free surface with the vessel in displacement mode.

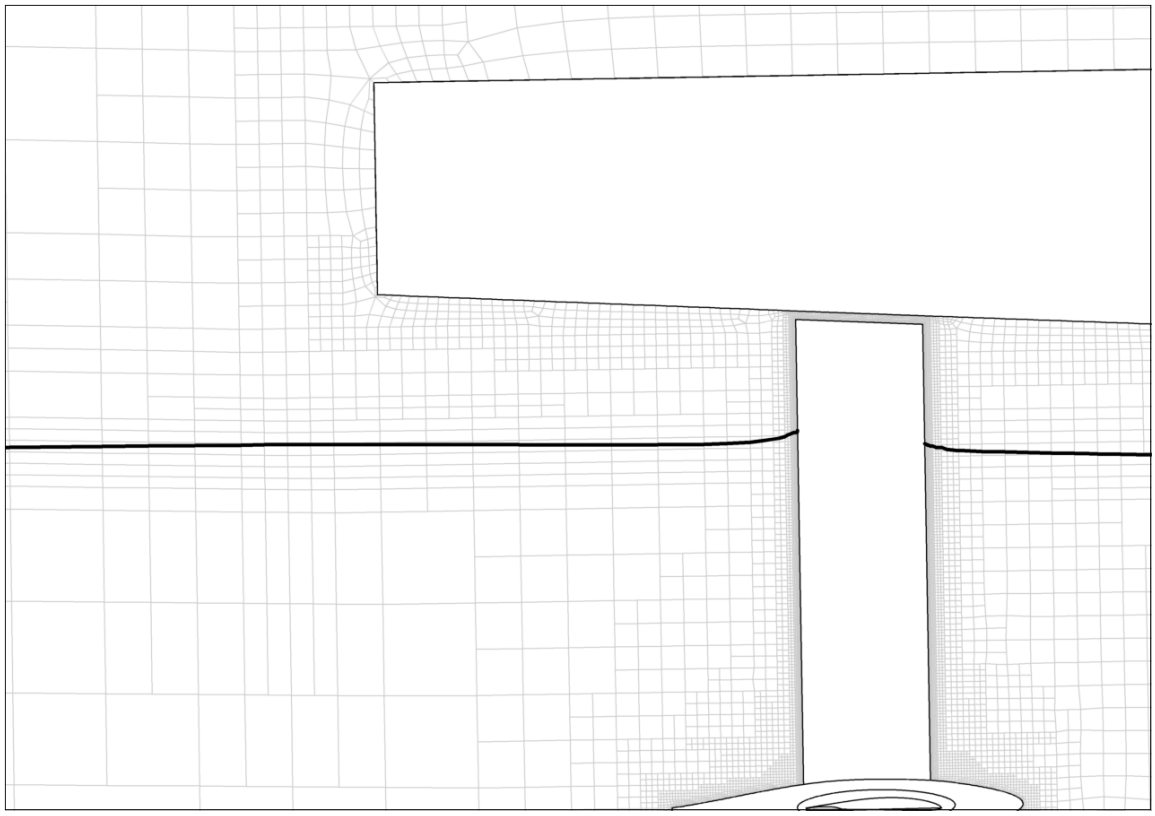

Fig. 4. The mesh at the free surface with the vessel in foiling mode.

2.2 Control strategy

The motion of each foil is controlled via so called 'dynamic libraries'. These control the motion of the foils as a function of variables resulting from the CFD computation. For each time step the pitch angle of the foils are computed and updated. The pitch angle is based on the trim and rise of the vessel.

The pitch angle of the forward foils is given by:

$$Rn_{fwd} = K_{p_{fwd}}\, e_{Tz0}(t) + K_{i_{fwd}} \int_0^t e_{Tz0}(t)dt \tag{7}$$

This means that the pitch angle of the forward foils is influenced by the sum of the proportional term and the integral term. The proportional term produces an output that is proportional to the magnitude of the current error. The integral term produces an output that is proportional to both the magnitude and the duration of the error. This takes in account the accumulated error over the past time. The error in the rise e_{Tz0} is given by:

$$e_{Tz0} = Tz0_{target} - Tz0 + Ry0 * 3.50 \tag{8}$$

Here $Tz0_{target}$ is the target rise at the location of the bow. The actual rise (at the bow of the vessel) is equal to $Tz0 - Ry0 * 3.50$ (bow-up trim is negative). Here the first term is the rise in the centre of gravity, and the second term is the trim multiplied by the distance between the centre of gravity (COG) of the vessel and the bow of the vessel. This accounts for the additional rise at the bow due to the dynamic trim of the vessel.

The pitch angle of the aft foils is given by:

$$Rn_{aft} = K_{p_{aft}}\, e_{Ry0}(t) + K_{i_{aft}} \int_0^t e_{Ry0}(t)dt \tag{9}$$

This means that the pitch angle of the aft foils is influenced by the sum of the proportional term and the integral term. The proportional term produces an output that is proportional to the magnitude of the current error. The integral term produces an output that is proportional to both the magnitude and the duration of the error. This takes in account the accumulated error over the past time. The error in the trim e_{Ry0} is given by:

$$e_{Ry0} = Ry0_{target} - Ry0 \tag{10}$$

Here the trim is set to a target value of $Ry0_{target}$. The actual trim is equal to $Ry0$. (bow-up trim is negative).

Both values for Rn_{fwd} and Rn_{aft} are limited to a range. These are bound by $Rn_{fwd_{min}}$ and $Rn_{fwd_{max}}$ for the forward foil and by $Rn_{aft_{min}}$ and $Rn_{aft_{max}}$ for the aft foil. If the calculated value exceeds these limits, the value will be set to this limit. This is to prevent excessively large pitch angles of the foils.

3. RESULTS AND DISCUSSION

This chapter provides the results of the analyses that were performed using the method described in chapter 2. In section 3.1 an overview of the employed control configurations is given followed by the results of these strategies. In section 3.3 the results are discussed.

3.1. Control configurations

The employed control strategies are based on the control strategy as described in section 2.2. An overview is given in table 2.

Table 2. Overview of employed control configurations

Parameter	Unit	configuration 1	configuration 2
$Tz0_{target}$	[m]	0.27	0.27
$K_{p_{fwd}}$	[-]	-45.0	-20.0
$K_{i_{fwd}}$	[-]	0.0	-5.0
$Rn_{fwd_{min}}$	[deg]	-8.0	-8.0
$Rn_{fwd_{max}}$	[deg]	3.0	3.0
$Ry0_{target}$	[deg]	0.0	0.0
$K_{p_{aft}}$	[-]	-2.5	-2.5
$K_{i_{aft}}$	[-]	0	-1.0
$Rn_{aft_{min}}$	[deg]	-8.0	-8.0
$Rn_{aft_{max}}$	[deg]	3	3

As can be observed from table 2, the first control configuration has proportional gain. The integration gain is equal to zero, therefore this is equal to a P-controller. The second control configuration has both proportional and integral gain, i.e. a PI-controller. To compensate for the contribution from the integrative action, the value for $K_{p_{fwd}}$ was lowered.

Both control configurations have the upper and lower bound for the foils set to 3 and -8 degrees respectively. This is done to prevent separation at the foils due to excessive pitch angles. It should be noted that a negative values for Rn_{aft} and Rn_{fwd} correspond to an increasing angle of attack.

In all analyses, the hydro-foiling vessel was accelerated in 10 seconds from a speed of 0 m/s to 8 m/s via an imposed acceleration profile.

3.2 Results

In the first part of this section the results are given for control configuration 1. In the second part of this section the results are given for control configuration 2.

3.1.1. Results for control configuration 1

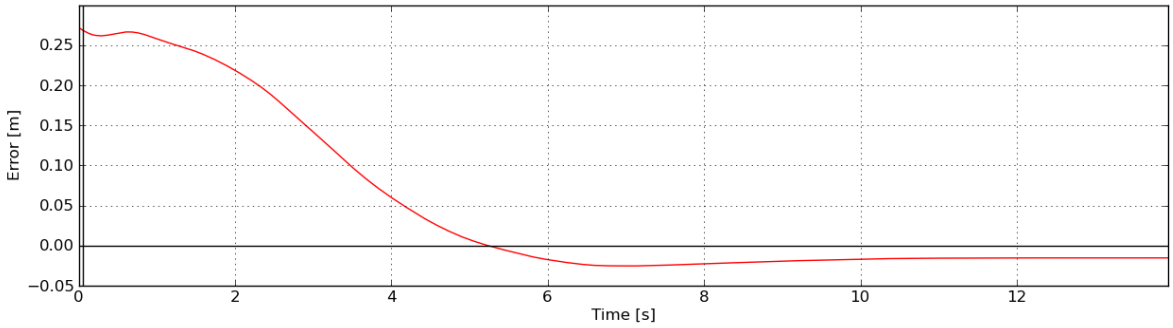

Fig. 5. e_{Tz0} as a function of time for the hydro-foiling vessel.

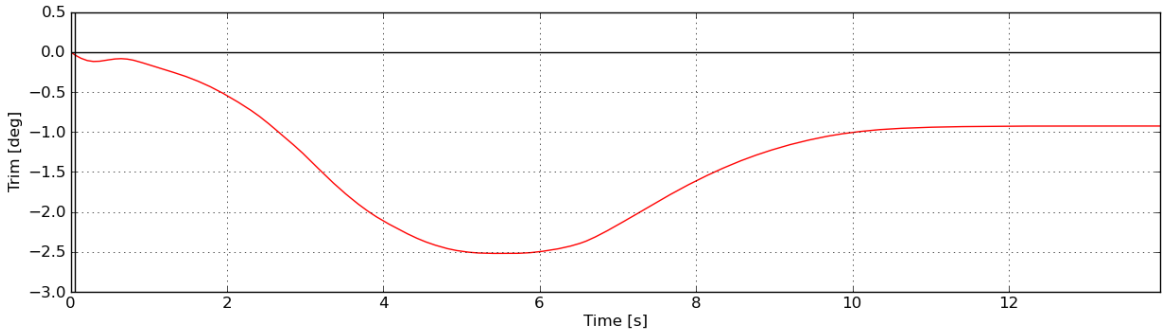

Fig. 6. $Ry0$ as a function of time for the hydro-foiling vessel.

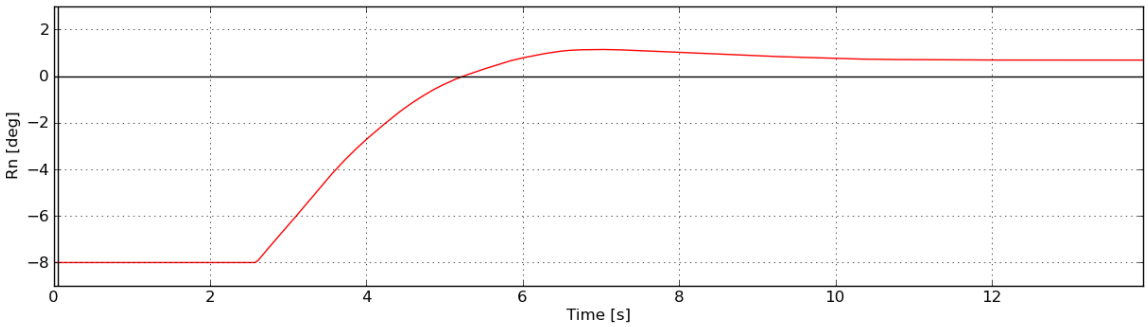

Fig. 7. Rn_{fwd} as a function of time for the hydro-foiling vessel.

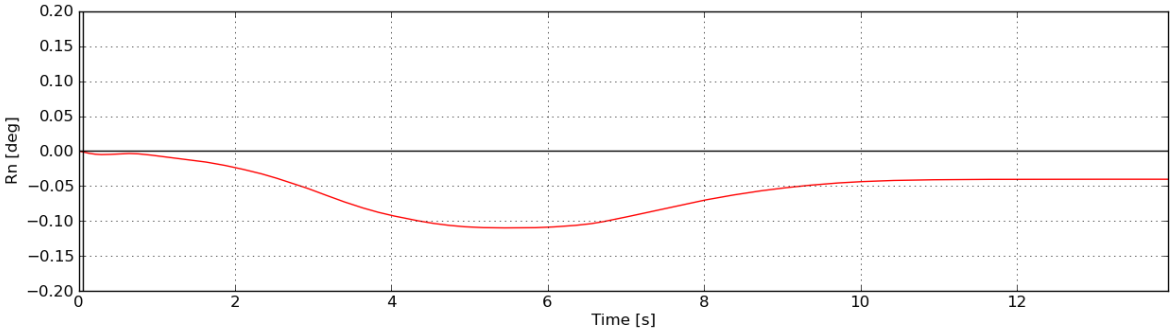

Fig. 8. Rn_{aft} as a function of time for the hydro-foiling vessel.

Figure 5 to 8 show the error in rise e_{Tz0}, the trim of the vessel (which is by definition -e_{Ry0}) and the pitch of the foils respectively. The vessel has reached its top speed after 10 seconds. After settling, the rise $Tz0$ has a value of 0.23 m. the trim has a value of -0.92°. This leads to an error e_{Tz0} of 0.015 m.

3.1.2. Results for control configuration 2

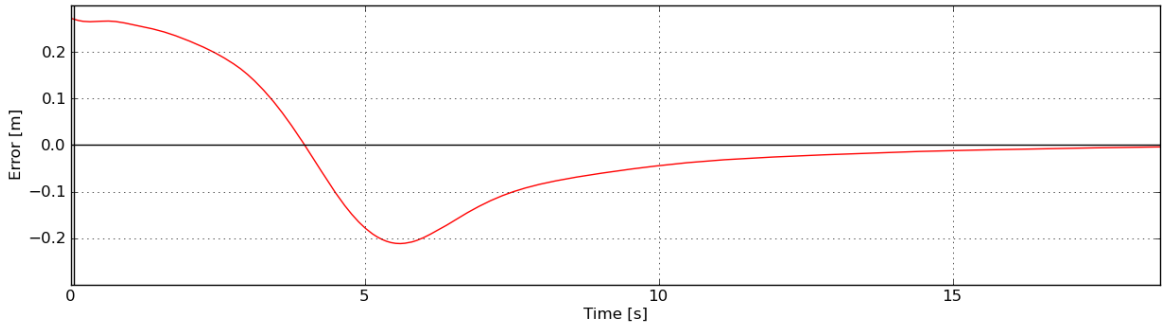

Fig. 9. e_{Tz0} as function of time for the hydro-foiling vessel.

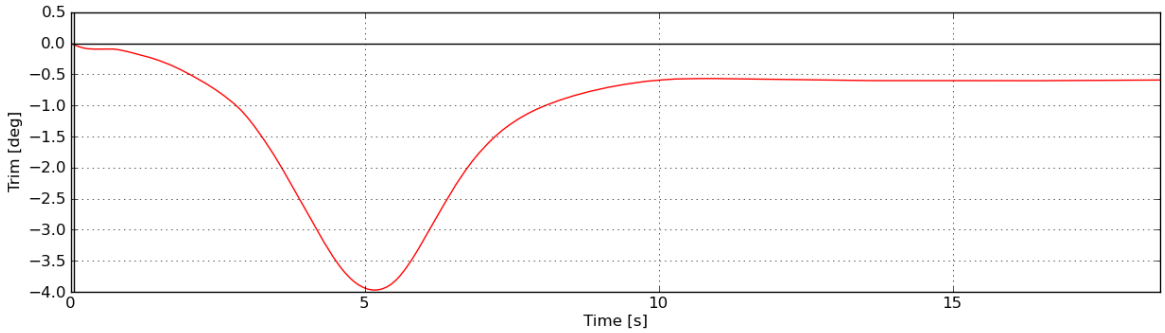

Fig. 10. $Ry0$ as a function of time for the hydro-foiling vessel.

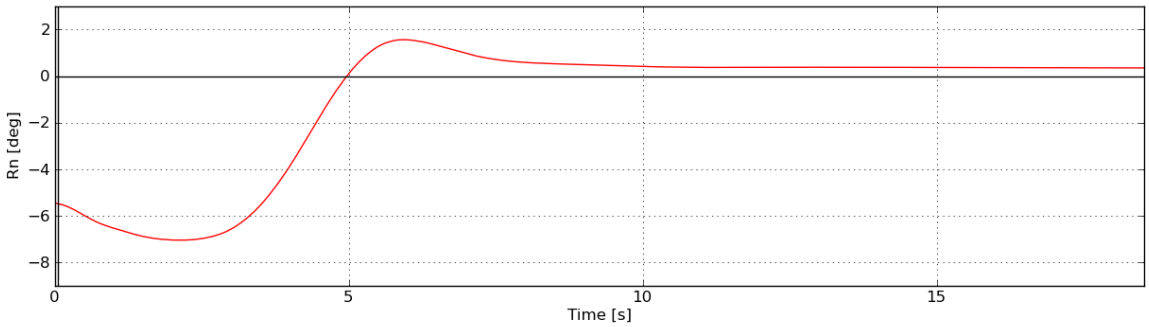

Fig. 11. Rn_{fwd} as a function of time for the hydro-foiling vessel.

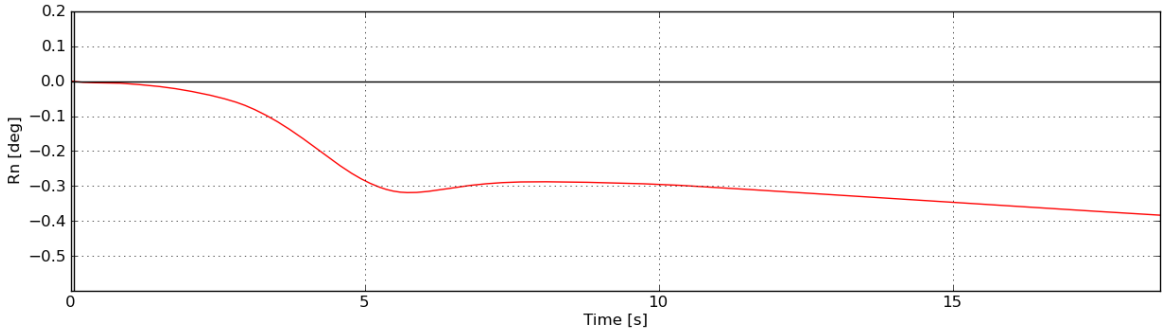

Fig. 12. Rn_{aft} as a function of time for the hydro-foiling vessel.

Figure 9 to 12 show the error in rise e_{Tz0}, the trim of the vessel (which is by definition -e_{Ry0}) and the pitch of the foils respectively. The vessel has reached its top speed after 10 seconds. After settling, the rise $Tz0$ has a value of 0.24 m. the trim has a value of -0.59°. This leads to an error e_{Tz0} of 0.004 m.

3.1.3. Discussion of the results

As can be seen the hydro-foiling vessel rises out of the water as intended for both control strategies. The results show a successful simulation of the transition from displacement mode to foiling mode for the present vessel where the vessel reacts as expected to the different control strategies.

For the control configuration 1 with the P-controller the following can be observed:

- An error is obtained of 0.015 meters.
- A constant e_{Tz0} error is obtained as shown in in figure 5. This is called droop, and is common for proportional controllers.
- For the first 2.5 seconds the forward foil has a constant pitch angle of -8 degrees. This can be observed in figure 7. The constant pitch is caused by the large error during this time frame in combination the large proportional gain $K_{p_{fwd}}$ This leads to a large pitch angle which is limited by the lower bound of pitch angle of the foil $Rn_{fwd_{min}}$.

For the control configuration 2 with the PI-controller the following can be observed:

- An error e_{Tz0} is obtained of 0.004 meters.
- The error e_{Tz0} goes to 0 asymptotically as shown in in figure 9. This behaviour is achieved by the integrative action of the PI-controller. The integrative action prevents the droop that is observed for control configuration 1.
- Due to the lower value for $K_{p_{fwd}}$ in control configuration 2 the lower bound for the forward foil pitch angle $Rn_{fwd_{min}}$ is not achieved.
- Overshoot can be observed in figure 9 and 10. This is caused by the integrative action and the slow response of the hydro-foiling vessel.
- From figure 12 it can be observed that the value for Rn_{aft} has not fully settled. This is caused by the still present error in the trim of the vessel. The integrative action of the PI-controller builds up the pitch angle of the aft foil until the error in the trim has asymptotically reached zero.

4. CONCLUSIONS

This paper demonstrates a method to study the control of the ride height and the trim of hydro-foiling vessels in RANSE based CFD computations. Using FINE/Marine the dynamic behaviour of the vessel was simulated. By using sliding grids pitch motion of the foils relative to the vessel was enabled. The changing free surface location, due to the large vertical translations of the vessel, was accurately resolved using Adaptive Grid Refinement (AGR).

Trim and rise of the vessel were controlled by adapting the pitch of the foils. Two control strategies, both based on a PID-controller as presented in section 2.2, were developed. The numerical method proved able to simulate the described control strategies.

The described method can be used for simulating and analysing complex ride height problems for a range of vessel. The future objective is to validate the method against test results from the vessel, and to improve the performance of the currently analysed solar boat.

ACKNOWLEDGEMENTS

The authors would like to thank J. Blom from the NHL Solarboat racing team for kindly providing the geometry for the presented analysis.

References

1. Menter F., "Zonal two-equations k-ω turbulence models for aerodynamic flows". AIAA paper 93-2906, 1993
2. Numeca International, User Manual FINE/Marine v3 (including ISIS-CFD), Numeca International, Brussels, Belgium, 2014
3. Queutey, P., Deng G., Wackers, J. and M. Visonneau, M., "Ventilated propeller simulation with a ranse solver", The 7th International Workshop on Ship Hydrodynamics, IWSH'2011, Shanghai, China,19 September 2011.
4. Queutey, P., Deng G., Wackers, J. "Coupled sliding grids and adaptive grid refinement for rans simulation of ship-propeller interaction," 14th Numerical Towing Tank Symposium, NUTTS'2011, Poole, United Kingdom, October, 2011.
5. Visonneau, M., Queutey, P., Deng, G., Guilmineau, E., Leroyer, A., and Mallol, B., "Computation of free surface viscous flows around self-propelled ship with the help of sliding grids," 11th International Conference on Computer Applications and Information Technology in the Maritime Industries, COMPIT'2011, Liege, Belgium, April, 2011.
6. Wackers, J., Deng, G., Leroyer, A., Queutey, P. and Visonneau, M., "Adaptive grid refinement for hydrodynamic flows", Computers & Fluids **55** (2012), 85-100
7. Dong Energy Solar Challenge, "Information folder", as retrieved from: http://www.dongenergysolarchallenge.com/uploads/Persdocumenten/Informationfolder%20DSC14-24June2014-lr.pdf, on 09th of September 2014
8. Dong Energy Solar Challenge, "History", as retrieved from: http://www.dongenergysolarchallenge.com/information/history, on 09th of September 2014